Imaging diffraction-limited electronic collimation from a non-equilibrium one-dimensional ballistic constriction



2000 J. Phys.: Condens. Matter 12 L167

(http://iopscience.iop.org/0953-8984/12/8/102)

J. Phys.: Condens. Matter **12** (2000) L167–L172. Printed in the UK PII: S0953-8984(00)10834-3

**LETTER TO THE EDITOR**

# Imaging diffraction-limited electronic collimation from a non-equilibrium one-dimensional ballistic constriction

R Crook, C G Smith, C H W Barnes, M Y Simmons and D A Ritchie
Department of Physics, Cavendish Laboratory, Madingley Road, Cambridge CB3 OHE, UK

Received 10 January 2000

**Abstract.** We report on the use of a low-temperature scanning probe microscope to investigate non-equilibrium electronic transport through a one-dimensional ballistic constriction. Transconductance images of electrons backscattered in the adjoining two-dimensional reservoirs show a weak acceptance cone consistent with semiclassical collimation. The images also show a strong highly collimated beam of quasi-particles injected into each reservoir with a divergence consistent with quantum mechanical diffraction. In the lower-chemical-potential reservoir these quasi-particles are interpreted as hot electrons while in the higher-chemical-potential reservoir they are interpreted as conduction-band holes.

A detailed understanding of conduction mechanisms in mesoscopic devices is a fundamental goal of condensed matter physics and continues to be an active topic of research [1]. With the advent of the split-gate patterning technique [2], experiments which investigate the way in which electrons flow through a constriction became possible. Magnetic steering experiments [3–7] have shown that electrons injected from such a constriction into an adjoining two-dimensional (2D) reservoir form a broad injection cone. Such observations were understood using a semiclassical transport theory [8] based on the assumption of non-adiabatic transport in the region where the constriction widens into a reservoir. The observation of ballistic one-dimensional (1D) quantization was a major advance in this field [9, 10] which confirmed the role of 1D subbands in determining conductance, considered in terms of quantum mechanical reflection and transmission coefficients [11]. Subsequent non-equilibrium measurements of 1D constrictions were also understood, within this formalism [12], to allow a determination of subband structure and energies. Although these experiments enable a comprehensive understanding of conduction though 1D constrictions to be achieved, they do not give any specific information about the spatial distribution of charge as it enters and relaxes into the 2D reservoirs.

We present experimental images of the trajectories of hot electrons and conduction-band holes (cb-holes) injected from a constriction or quasi-one-dimensional electron system (Q1DES) into an adjoining 2D reservoir or two-dimensional electron system (2DES). A cb-hole is a hole-like quasi-particle in the conduction band with an energy less than the Fermi energy, which is equivalent to an unoccupied electron state. In addition to the expected semiclassical collimation cone, the images reveal highly collimated beams of hot electrons or cb-holes with a divergence that is not explained by the semiclassical theory [8]. In the experiment, the scanning charged tip of a low-temperature atomic force microscope (AFM) locally perturbs the 2DES electrostatic potential adjacent to a Q1DES which exhibits clear conductance quantization. As previously demonstrated [13–15], the tip perturbation can backscatter transmission electrons,

0953-8984/00/080167+06$30.00  

such that images of the Q1DES transconductance reveal the ballistic electron flux and trajectory. We extend this method by applying a larger source–drain bias $V_{sd}$ across the Q1DES. By choosing $V_{sd}$ an order of magnitude greater than $k_B T$, we make the hot electrons and cb-holes isolated from the Fermi sea.

The Q1DES exists in a high-mobility 2DES layer created at a $GaAs/Al_xGa_{1-x}As$ heterojunction 98 nm beneath the device surface†. After illumination with a red light-emitting diode, the 2DES has a low-temperature mobility of 300 $m^2\ V^{-1}\ s^{-1}$ and a carrier density of $2.4 \times 10^{11}\ cm^{-2}$ giving an electron mean free path of 25 $\mu$m. A negative bias applied to surface electrodes depletes underlying 2DES electrons to define the Q1DES. The surface electrodes are in a split-gate configuration, with a lithographic Q1DES width of 700 nm and length of 400 nm.

Our AFM, which operates at 1.5 K, uses a piezoresistive cantilever [16]‡ to sense the force on the tip, which avoids the complications of making optical measurements of deflection at low temperatures. We locate the surface electrodes and Q1DES using the AFM in the conventional force-sensing mode. The images presented in this letter are transconductance images where an AC signal is applied to the conductive AFM tip scanning a few nm above the device surface. The AC component of the Q1DES conductance, which is referred to as the transconductance $G_t$, is recorded in synchrony with the scanning tip to determine the image contrast. The images do not cover the 30 nm thick surface electrodes, to avoid a collision with the tip movement.

Figure 1(a) plots $G_t$§ as a function of gate bias $V_g$ with a 0.5 $V_{rms}$ AC signal applied to the tip. Although the tip was positioned 1 $\mu$m from the constriction, the AC signal on the cantilever (which supports the tip) perturbed the background electrostatic potential. Each peak in figure 1(a) corresponds to a change in 1D subband index, demonstrating that seven subbands can be identified at 1.5 K. With the gates biased to transmit five subbands, the tip was scanned 10 nm off the device surface to generate the transconductance image shown in figure 1(b).

A wide cone enclosed by dashed lines which diverge at $\alpha_{max} \approx \pm 34^\circ$ is identified in figure 1(b), and interpreted as the semiclassical cool-electron acceptance cone [8]. This cone defines the angular distribution of electrons to be transmitted through the constriction. The centre of the cone is offset from the centre of the lithographically defined split-gate pattern, probably owing to device inhomogeneities. The tip electric field locally perturbs the 2DES electrostatic potential, the perturbation being largest in the negative half-cycle of the AC tip bias. If the tip perturbation scatters electrons that would have otherwise been transmitted, then the transconductance is reduced as observed in figure 1(b). The semiclassical acceptance cone, bounded by $\pm\alpha_{max}$, is governed by the raised potential associated with the Q1DES, and also by the potential geometry at the Q1DES entrance. The adiabatic invariance of $W|k_y|$ provides [8]

$$\alpha_{max} = \arcsin\left(\sqrt{\frac{E_F - E_b}{E_F}}\frac{W_{min}}{W_{max}}\right) \tag{1}$$

where $E_b$ is the maximum raised potential which occurs at the minimum Q1DES width $W_{min}$, and $E_F$ is the 2DES electron Fermi energy. Beyond $W_{max}$, transport becomes non-adiabatic, although numerical calculations have shown that this transition is not abrupt [4]. The semiclassical injection cone is similarly bounded by $\pm\alpha_{max}$, although $E_b$ will differ by $eV_{sd}$.

Figure 1(b) also reveals a bright central beam, enclosed by dotted lines that diverge at approximately $\pm 3^\circ$. A convolution of the width of the Q1DES and the width of the tip perturbing potential [14] defines the minimum width of the central beam. Scattering of electrons

† Cavendish wafer T32.

‡ Park Scientific Instruments, Sunnyvale, CA 94089, USA.

§ The AC signal is applied to the tip while the gate bias is swept, so $G_t$ is proportional to $dG/dV_g$.

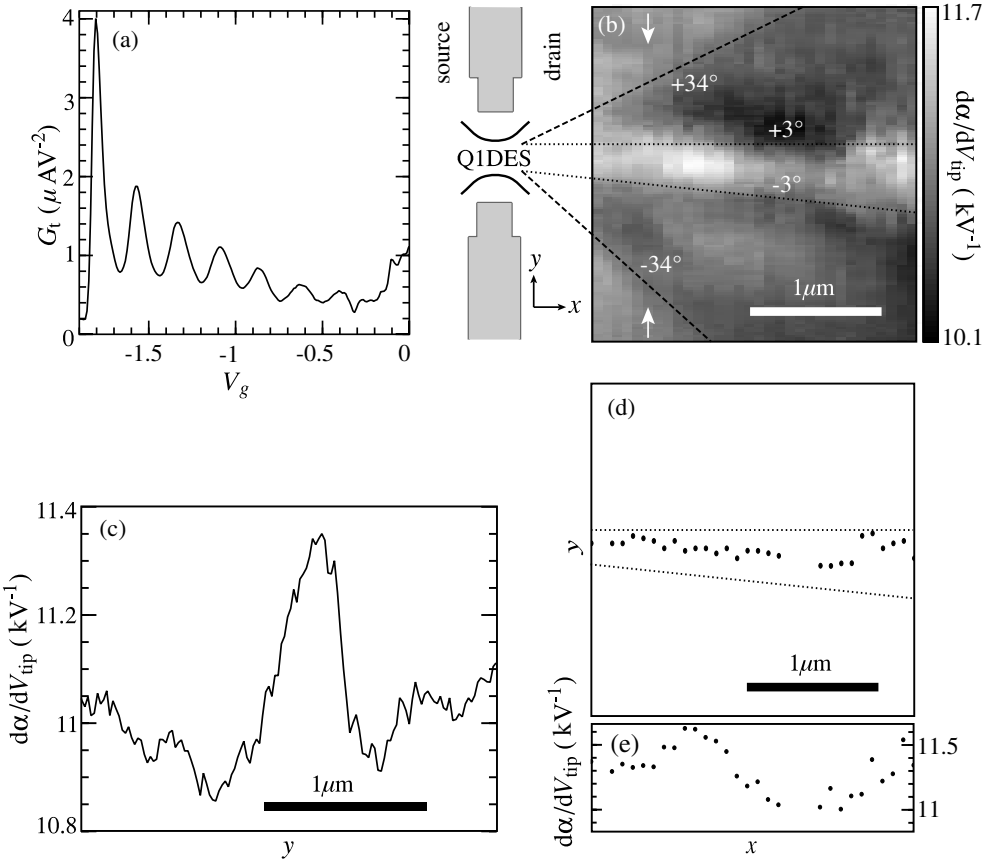


**Figure 1.** (a) A plot of Q1DES transconductance against gate bias at $V_{sd} = -0.1$ mV. (b) A transconductance image at $B = 0$ T, and $V_{sd} = -1$ mV. The dashed lines enclose a $\pm 34^\circ$ cone, while the dotted lines enclose a $\pm 3^\circ$ beam. The positions of the surface electrodes and Q1DES are shown. (c) A profile of a single line from image (b), where it is identified by arrows. (d) Spatially corresponding maxima of image (b). (e) Maximum transconductance against $x$, from image (b). Backscattered ratio $\alpha \equiv I_{\text{backscattered}}/I_{\text{transmitted}}$. All measurements were made at 1.5 K.

back through the Q1DES reduces the conductance, but increases the transconductance as observed. Such extreme collimation has not been previously reported and is not predicted for semiclassical collimation.

Figure 2 shows transconductance images made in weak perpendicular magnetic fields, to study magnetic steering of the quasi-particle beams. The solid lines shown on the images are the calculated cyclotron trajectories for electrons at the 2DES Fermi energy in magnetic fields of $\pm 2.4$ mT. The hot-electron beams of figures 2(a) and 2(c), where $V_{sd} = -2$ mV, are deflected along an approximately circular path to coincide with the calculated cyclotron trajectory where $r_c = 34\ \mu$m. The dashed lines in figure 2 are experimental lines of maximum transconductance†, while the dotted lines show the quarter-maximum transconductance to indicate the width of the beam. The extended cyclotron trajectories do not intersect at the Q1DES centre, but are laterally offset by about $\pm 50$ nm at the Q1DES entrance. The Lorentz

† In figures 2(b) and 2(d) the greyscale shows negative transconductance in order to identify the negative source–drain bias used for these images.

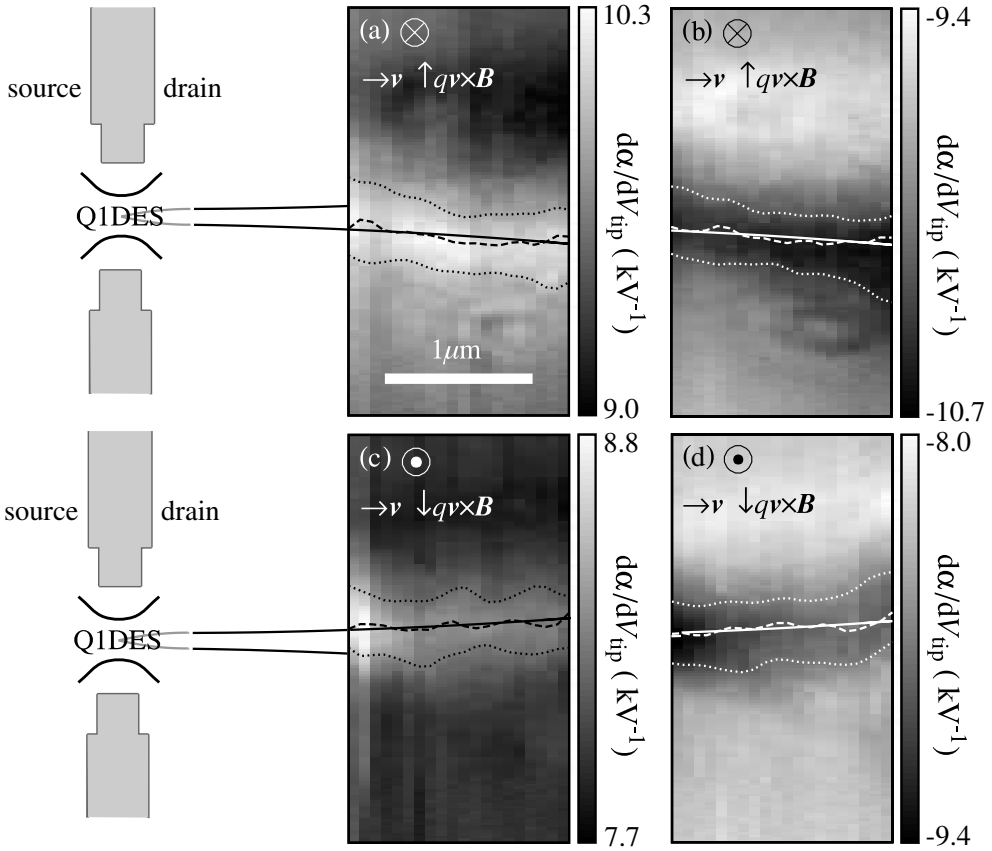


**Figure 2.** Transconductance images. In (a) and (b), $B = +2.4$ mT; in (c) and (d), $B = -2.4$ mT. In (a) and (c), $V_{sd} = -2$ mV; in (b) and (d), $V_{sd} = +2$ mV. Dashed lines follow the maximum transconductance, dotted lines enclose the quarter-maximum range of transconductance, and solid lines are best-fit cyclotron trajectories for $r_c = 34$ $\mu$m. The surface electrodes are shown in (a) and (c) only. Backscattered ratio $\alpha \equiv I_{\text{backscattered}}/I_{\text{transmitted}}$.

force for a small longitudinal momentum modifies the path in the Q1DES. Backscattering of hot electrons still occurs as the magnetic deflection is sufficiently small for there to be states available for the backscattered hot electrons to be transmitted. Indeed, in increasing magnetic fields the structure in the images rapidly diminishes.

In figure 2(b) and 2(d), $V_{sd} = +2$ mV. Although there are no hot electrons, a highly collimated beam is still observed. Such beams can be regarded as the backscattering of a beam of cb-holes. The backscattered cb-hole flux reduces the Q1DES conductance, so again the transconductance increases†. cb-holes have a positive charge, but because the conduction-band dispersion curve has a positive curvature, they have negative effective mass and are therefore magnetically steered in the same direction as hot electrons. Indicated on the images of figure 2 are the quasi-particle direction $\boldsymbol{v}$ and the direction of the Lorentz force $q\boldsymbol{v} \times \boldsymbol{B}$ for a positive charge $q$. A beam of valence-band holes would be steered in the direction opposite to that observed, as would the scattering of electrons destined to become the hot-electron beam on

† In figures 2(b) and 2(d) the greyscale shows negative transconductance in order to identify the negative source–drain bias used for these images.

the other side of the Q1DES. A beam of electrons backscattered on this more negative side of the Q1DES would cause increased conductance and decreased transconductance, which is not observed†. There exist empty states available for backscattered hot electrons, and occupied states available for backscattered cb-holes.

The cb-hole is a hole-like quasi-particle that exists in the conduction band with an energy less than $E_F$. A cb-hole is generated in the Q1DES simultaneously with a hot electron, making a cb-hole–hot-electron pair. The hot electron is accelerated towards the lower chemical potential while the cb-hole is accelerated towards the higher chemical potential. The tip perturbing potential scatters cb-holes when an electron occupying a state of different momentum is scattered into the cb-hole state, so leaving the electron state unoccupied, and thus a cb-hole. Alternatively, the cb-hole can be considered as an unoccupied electron state, but the discussion becomes less concise.

We interpret the ring-shaped feature, prominent in the lower right region of figures 2(a) and 2(c), as the effect of scanning the tip over a defect. The defect causes a local inhomogeneity in the 2DES electrostatic potential, and is positioned just outside the narrow beam but inside the cool-electron injection and acceptance cones. The scattering effect and origin of the defect are uncertain.

We interpret the bright central beam seen in the image of figure 1(b) as a hot-electron beam. At the centre of the Q1DES all the transmission electrons occupy a few 1D subbands with well defined lateral momentum $\hbar k_x$. Away from the centre, transport remains adiabatic, so $k_x$ for the transmission electrons will increase. Where the Q1DES widens into the 2DES, the subband spacing approaches zero and adiabatic transport breaks down. Most transmission electrons scatter and preserve their $k_x$ into the 2DES with a limit on the minimum $k_x$, and an associated limit on the maximum $|k_y|$, to produce the semiclassical injection cone of equation (1). However, for the 'lucky' electrons that remain adiabatic furthest away from the Q1DES, $k_x$ continues to increase towards $k_F$, so $|k_y|$ is necessarily small and thus the highly collimated hot-electron beam is formed. This is equivalent to the limit $W_{max} \rightarrow \infty$ in equation (1). This experiment is sensitive to these lucky electrons because to contribute to the transconductance measurement the electrons must be scattered back through the same Q1DES. The lucky electrons which are backscattered and remain adiabatic into the Q1DES will occupy the states of largest $|k_x|$, which are the states that will become the few occupied subbands at the Q1DES centre, and hence a highly collimated beam is observed. Other electrons which are scattered back towards the Q1DES will occupy states of lower $|k_x|$ near the Q1DES and are therefore reflected and not transmitted. Highly collimated beams of cb-holes were also observed. To return through the Q1DES the cb-holes must remain adiabatic and so $|k_x|$ increases to near $k_F$ and a narrow beam is observed in analogy to the hot-electron beam.

The uncertainty principle applied at the Q1DES centre sets the minimum beam divergence, so $|\Delta y\, \Delta k_y| \geqslant 1$. For our device $\Delta y = W \approx 200$ nm giving $\Delta k_y \geqslant 5 \times 10^6$ m$^{-1}$. The 2DES Fermi energy was $E_F = 8.5$ meV, so from the dispersion relation $k_x^2 + k_y^2 = 2m^* E_F/\hbar^2$, quantum mechanical diffraction limits the collimation to a minimum of $\pm 2.3^\circ$, somewhat less than the $\pm 3^\circ$ divergence seen in figure 1(b). Along the length of the beam, the transconductance should decay exponentially, so in principle a hot-electron mean free path can be deduced. Figure 1(e) shows the maximum transconductance along the length of the beam. Other structure dominates, probably originating from disorder in the 2DES electrostatic potential arising from the random distribution of dopants [17].

Alternatively, the structure seen in the images could be a projection of the electrostatic

† In figures 2(b) and 2(d) the greyscale shows negative transconductance in order to identify the negative source–drain bias used for these images.

disorder in the vicinity of the Q1DES. Near the Q1DES, the 2DES screening is reduced, so disorder becomes significant enough to determine the beam structure. In the bulk 2DES where backscattering occurs, 2DES screening of donor disorder is significant, so the beam is not modified. The image of figure 1(b) appears symmetric about the Q1DES longitudinal axis, which suggests that this alternative theory is not complete, although it may explain the misalignment between the cone and the beam. The images may instead be a manifestation of the electron–electron scattering process as the injected beam decays in the 2D reservoir. Buhmann and Molenkamp [18] predict a beam of electrons antiparallel to the primary beam, and a very narrow beam of cb-holes in the forward direction.

In conclusion, we have produced transconductance images of hot-electron and conduction-band-hole (cb-hole) trajectories using a novel low-temperature scanning probe microscope. The hot electrons and cb-holes were generated in a Q1DES with a dc source–drain bias of magnitude 2 mV, then accelerated in opposite directions several microns into a 2DES. We observed beams with a width limited by the scanning tip perturbation, implying a beam divergence of less than $\pm 3^\circ$. The highly collimated beams are believed to be caused by those electrons and cb-holes which remain adiabatic and coherent throughout the Q1DES and into the 2DES. The divergence of the beam may be limited by quantum mechanical diffraction which was calculated as $\pm 2.3^\circ$ for this experiment. The cb-hole is not normally considered in non-equilibrium transport through a Q1DES. These experiments highlight the symmetry of hot-electron–cb-hole generation and the equal importance of the cb-hole as a charge carrier. Such an interpretation suggests a new approach to formulating models of Q1DES transport.

We thank C J B Ford and J T Nicholls for helpful discussions. We acknowledge financial support from the EPRSC and from the RW Paul Instrument Fund. CHWB and DAR thank the EPSRC and Toshiba Research Europe Limited respectively.

## References

[1] For a comprehensive review, see Kelly M J 1995 *Low-Dimensional Semiconductors* ed H Kamimura, R J Nicholas and R H Williams (Oxford: Clarendon)
[2] Thornton T J *et al* 1986 *Phys. Rev. Lett.* **56** 1198
[3] Wharam D A *et al* 1988 *J. Phys. C: Solid State Phys.* **21** L887
[4] Molenkamp L W *et al* 1990 *Phys. Rev.* B **41** 1274
[5] Molenkamp L W, Brugmans M J P, van Houten H and Foxon C T 1992 *Semicond. Sci. Technol.* **7** 228
[6] Cumming D R S, Ahmed H and Thornton T J 1992 *Appl. Phys. Lett.* **60** 2755
[7] Okada M *et al* 1992 *Semicond. Sci. Technol.* **7** 223
[8] Beenakker C W J and van Houten H 1989 *Phys. Rev.* B **39** 10 445
[9] van Wees B J *et al* 1988 *Phys. Rev. Lett.* **60** 848
[10] Wharam D A *et al* 1988 *J. Phys. C: Solid State Phys.* **21** 209
[11] Landauer R 1957 *IBM J. Res. Dev.* **1** 223
[12] Martin-Moreno L, Nicholls J T, Patel N K and Pepper M 1992 *J. Phys. C: Solid State Phys.* **4** 1323
[13] Eriksson M A *et al* 1996 *Appl. Phys. Lett.* **69** 671
[14] Crook R *et al* 1999 *Proc. 24th Int. Conf. on the Physics of Semiconductors* ed D Gershoni (Singapore: World Scientific) p 190
Crook R *et al* 1999 *e-print* cond-mat/9909017
[15] Crook R *et al* 2000 *Physica* E **6** 234
[16] Tortonese M, Barret R C and Quate C F 1993 *Appl. Phys. Lett.* **62** 834
[17] Nixon J A and Davies J H 1990 *Phys. Rev.* B **41** 7929
[18] Buhmann H and Molenkamp L W 1998 *Low Temp. Phys.* **24** 737